



Published in final edited form as:

J Leukoc Biol. 2026 February 09; 118(2): . doi:10.1093/jleuko/qiaf174.

RABEP1 Regulates Neutrophil Migration via Endosomal Recycling and Actin Polymerization

Daniel H. Kim^{1,§}, Ramizah Syahirah^{1,§,#}, Conwy Zheng¹, Chang Ding¹, Alan Y. Hsu^{1,&}, Tyler Pikes¹, Zhaolun Liang¹, Sheng Liu^{2,3}, Linlin Li⁴, Xiaoping Bao^{5,6}, David Umulis⁴, Jun Wan^{2,3,7}, Qing Deng^{1,6,*}

¹Department of Biological Sciences, Purdue University, West Lafayette, Indiana, USA.

²Department of Medical and Molecular Genetics, Indiana University School of Medicine, Indianapolis, IN, 46202, USA.

³Collaborative Core for Cancer Bioinformatics, Indiana University Simon Cancer Center, Indianapolis, IN, 46202, USA.

⁴Weldon School of Biomedical Engineering, Purdue University, West Lafayette, IN 47907, USA.

⁵Davidson School of Chemical Engineering, Purdue University, West Lafayette, IN 47907, USA.

⁶Institute for Cancer Research, Purdue University, West Lafayette, IN 47907, USA.

⁷Center for Computational Biology and Bioinformatics, Indiana University School of Medicine, Indianapolis, IN, 46202, USA.

Abstract

Neutrophils are the first responders of our innate immune system, crucial for defense against various infections. The intricate regulation of neutrophil migration is essential for neutrophil function. However, a complete mechanistic understanding is missing. We previously performed a miRNA overexpression screen and identified miR-190 as a potent suppressor of neutrophil migration in zebrafish. Through a second round of small-scale screening using neutrophil-specific knockouts of putative miR-190 targets, we identified that *rabep1* (encoding Rabaptin, RAB GTPase Binding Effector Protein 1) is essential for neutrophil motility and chemotaxis in zebrafish. Re-expressing full-length Rabaptin, but not its truncation lacking the Rab4/Rab5 binding domain, rescued cell motility in the knockout. Knocking down *RABEP1* in differentiated human leukemia (dHL-60) cells consistently reduced cell motility. RABAPTIN-deficient dHL-60 cells are defective with fast recycling, yet maintain a normal Rab5 GTP level. The RABAPTIN-

*Corresponding author: Qing Deng, 915 Mitch Daniels Blvd, West Lafayette, IN 47907. qingdeng@purdue.edu.

#present address: Regenerative Medicine Institute, Cedars-Sinai Medical Center, Los Angeles, California, USA.

&present address: Department of Pathology, Harvard Medical School, Boston, Massachusetts, USA./Department of Laboratory Medicine, The Stem Cell Program, Boston Children's Hospital, Boston, Massachusetts, USA.

§DHK and RS contributed equally to this work

Authorship Contribution Statement

DHK: Conceptualization, investigation, data analysis, and writing of the manuscript. RS: Investigation, data analysis, and editing of manuscript. CZ, SL, LL, TP, ZL, AYH: Investigation, data analysis. JW, UM: supervision. XB: Resources. QD: Conceptualization, supervision, funding acquisition, and writing of the manuscript.

Competing interests

The authors declare no competing interests.

deficient cells displayed reduced PAK phosphorylation and decreased F-actin levels, yet still appropriately polarized upon chemokine stimulation. Overexpression of dominant-negative Rab4 or Rab5 has a similar inhibitory effect on neutrophil migration. Our data suggest that RABAPTIN drives endosomal recycling, Rac activation, and leading-edge actin polymerization, providing significant insights into the role of the endocytic pathway in neutrophil motility.

Summary sentence:

Rabaptin facilitates fast endosomal recycling, which activates Rac-PAK signaling and reinforces actin polymerization at neutrophil front to support motility.

Keywords

Rabep1; miR-190; zebrafish; HL-60 cells; endocytic pathway

Introduction

Neutrophils are essential innate immune cells that respond to infections and inflammation.¹⁻² Neutrophils migrate to inflammation sites, expressing and releasing cytokines to recruit other cells of the immune system while also directly attacking foreign microorganisms through degranulation, phagocytosis, the production of reactive oxygen species (ROS), and the generation of neutrophil extracellular traps.³⁻⁵ However, deregulated neutrophil functions can lead to various diseases, including inflammatory diseases, autoimmune diseases, and cancer.⁶⁻⁸ Therefore, the regulation of neutrophil migration is essential to maintain a balanced and efficient immune system.⁹⁻¹¹ The specific molecules involved in modulating neutrophil migration, or the exact mechanisms behind such regulation, are not yet well understood. MicroRNAs (miRNAs) are short, conserved, non-coding RNAs that function as regulators of the transcriptome.¹² They bind to their target genes' 3' untranslated regions and recruit the RNA-induced silencing complex, downregulating their expression.¹³⁻¹⁴ Until now, most miR studies have been conducted using transgenic mouse models, with only a handful focused on neutrophil functions, including migration. This approach, however, entails limitations such as difficulty visualizing neutrophil motility in vivo and non-conclusive results due to non-specific inflammation induced by invasive methods for imaging.¹⁵⁻¹⁶ To overcome such limitations, we have utilized the zebrafish model, which shares a highly similar immune system with mammals. It also supports noninvasive live imaging since zebrafish are transparent through their embryonic and larval stages.¹⁷⁻²⁰

Our previous study, which screened a wide array of miRs, identified nine hits that significantly decreased neutrophil chemotaxis to a tail wound or bacterial ear infection site when overexpressed in zebrafish neutrophils.²¹ We expanded these initial findings to focus on a specific defect of cell motility. Subsequently, we screened putative *miR-190* target genes using neutrophil-specific knockout²² and thereby identified *Rabep1* that is specifically required for neutrophil motility.

Rabep1 is the protein-coding gene for Rabaptin, RAB GTPase Binding Effector Protein 1, which acts as an effector for Rab4 and Rab5.²³ Rab family proteins control vesicular trafficking, a process vital for cell migration by activating signaling pathways or by internalizing and recycling receptors.²⁴⁻²⁶ However, it has not been determined whether endosomal recycling influences neutrophil migration. To explore this, we examined the phenotype of *RABEP1* knockdown in dHL-60 cells. The RABAPTIN-deficient cells showed impaired motility, with an excess of internalized endosomes and decreased Rac activation, indicating that RABAPTIN is crucial for endosome recycling and the precise regulation of neutrophil migration.

Methods

Reagents

ATCC Universal Mycoplasma Detection Kit (ATCC, 50-238-3275), HBSS (Gibco, 14025-092), Puromycin (Gibco, A1113803), Penicillin-Streptomycin (Gibco, 15140122), GlutaMax (Gibco, 35050-0611), OPTI-MEM (Gibco, 51985-034), pHrodo™ Green *E. coli* BioParticles™ Conjugate (Invitrogen, P35366), Amplex Red Hydrogen Peroxide Peroxidase Assay Kit (Invitrogen, A22188), eBioscience™ Flow Cytometry Staining Buffer (Invitrogen, 00-4222-26), Novex™ Tris-Glycine SDS Running Buffer (Invitrogen, LC26754), Pierce™ 10X Western Blot Transfer Buffer (35040), PageRuler™ Prestained Protein Ladder (26616), RIPA Lysis and Extraction Buffer (89900), Pierce™ Protease Inhibitor Tablets (A32965), Lipofectamin 3000 Transfection Kit (L3000015), PVDF Transfer Membranes (88518), 10 x PBS (BP3994), Sudan Black (BP109-10), DMSO (327182500), TEMED (BP150-20), Ammonium Persulfate (17874), Agarose (BP160-500), 20 x TBS Tween20 (28360), Tween20 (AAJ20605AP), Triton X-100 (AAA16046AP), Bovine Serum Albumin (BP1600-100), KOH (437135000), NaCl (BP358-1), Sodium Phosphate (BP332-500), KCl (BP366-500), CaCl₂ (C79-500), MgSO₄ (BP213-1) and H₂O₂ (H325-500) were from ThermoFisher Scientific (Waltham, MA, USA). dPBS (21-031-CV), RPMI-1640 (10-041-CV), DMEM (10-013-CV), HEPES (25-060-CI), Falcon® 12-well Clear Flat Bottom TC-treated Multiwell Cell Culture Plate (353043), Corning® 100 mm Not TC-treated Culture Dish (430591), Falcon® 100 mm TC-treated Cell Culture Dish (353003), Falcon® 96-well Cell Clear Flat Bottom TC-treated Culture Microplate (353075), Sodium Bicarbonate (25-035CI) and Sodium Pyruvate (25-000-CI) were from Corning (Corning, NY, USA). MISSION® TRC2 pLKO.5-puro Non-Mammalian shRNA Control Plasmid DNA (SHC202), MISSION® pLKO.1-puro-CMV-TurboGFP™ Positive Control Plasmid DNA (SHC003), MISSION® TRC2 pLKO.5-puro *RABEP1* shRNA 1 Plasmid DNA (TRCN0000327713), MISSION® TRC2 pLKO.5-puro *RABEP1* shRNA 2 Plasmid DNA (TRCN0000363576), MISSION® TRC2 pLKO.5-puro *RABEP1* shRNA 3 Plasmid DNA (TRCN0000369958), glucose (G8270-100G), Fibrinogen (F3879), polybrene (TR-1003-G), PMA (P1585), TCA (T6399), NaF (G9422), β-glycerophosphate (S6776) and fMLP (F3506) were from Millipore Sigma (Burlington, MA, USA). 30% Acrylamide/Bis Solution (1610156), 10% SDS Solution (1610416), 2× Laemmli sample buffer (1610737), Resolving Gel Buffer (1610798) and Stacking Gel Buffer (1610799) were from Bio-Rad Laboratories (Hercules, CA, USA). PrimeSTAR MAX DNA Polymerase (R045), In-Fusion® Snap Assembly Master Mix (ST2320), SOC media (ST0215), Lenti-X concentrator (631232) and

Stellar™ Competent Cells (636763) were from Takara Bio (San Jose, CA, USA). Plasmids pCMV-dR8.2 dvpr (8455), pCMV-VSV-G (8454), Rab5DN (35139), Rab5 CA (35140), TagRFP-T-EEA1 (42635) were from Addgene (Watertown, MA, USA). Geneblocks for Rab4 DN and Rab11 DN were from Twist Biosciences (San Francisco, CA, USA). Versaladder DNA ladder (D012-500) and Low Melt Agarose (A-204-25) were from GoldBio (St. Louis, MO, USA). Ibidi μ -Slide 8 Well High ibiTreat (80806) and μ -Slide 8 Well High Glass Bottom (80807) were from IBIDI (Fitchburg, WI, USA). Leukotriene B₄ (20110) was from Cayman Chemicals (Ann Arbor, MI, USA). HyClone™ Characterized Fetal Bovine Serum (SH30396.03) was from Cytiva (Marlborough, MA, USA). VECTASHIELD HardSet Antifade Mounting Medium (H-1400-10) was from VectorLabs (Newark, CA, USA). Paraformaldehyde Solution (15710) was from Electron Microscopy Sciences (Hatfield, PA, USA). The Human *RABEPI* cDNA Clone (HG19536-ACGLN) was obtained from Sino Biological (Wayne, PA, USA). Rab5 Pull-Down Activation Assay Kit (83701) was from NewEast Biosciences (King of Prussia, PA, USA). Black Wall 96-well Plate (655096) was from Greiner Bio-One (Monroe, NC, USA). Ethanol 200 Proof (2701) was from Decon Labs (Bryn Mawr, PA, USA). Precision Red Advanced Protein Assay (ADV02) was from Cytoskeleton, Inc. (Denver, CO, USA). Antibodies for immunoblotting were anti-*RABEPI* (HPA019669-25ul), anti-Vinculin (V9264), and anti- α -Tubulin (T5168) from Millipore Sigma (Burlington, MA, USA). Phospho-PAK1 (Ser199/204)/PAK2 (Ser192/197) Antibody (2605S) and PAK2 (3B5) Mouse mAb (4825S) from Cell Signaling (Danvers, MA, USA); secondary antibodies used were: Goat anti-Mouse IgG (H+L) Secondary Antibody (DyLight™ 680) (Invitrogen, 35518), Goat anti-Rabbit IgG (H+L) Secondary Antibody (DyLight™ 800 4X PEG) (Invitrogen, SA535571) from ThermoFisher Scientific (Waltham, MA, USA). Antibodies for immunofluorescence were Wheat Germ Agglutinin (Invitrogen, W32465), Transferrin From Human Serum, Alexa Fluor™ 488 Conjugate (Invitrogen, T13342), Alexa Fluor™ 488 Phalloidin (Invitrogen, A12379), and DAPI (Invitrogen, D3571) from ThermoFisher Scientific (Waltham, MA, USA). Phospho-Myosin Light Chain 2 (Ser19) Mouse mAb (3675) from Cell Signaling (Danvers, MA, USA); secondary antibodies used were: Goat anti-Mouse IgG (H+L) Secondary Antibody, DyLight™ 680 (Invitrogen, 35518). Antibodies for flow cytometry were BD Horizon™ BV421 Annexin V (BDB563973) and anti-Mouse IgM, κ Isotype Control (BDB562704) from BD Biosciences (San Jose, CA, USA). Alexa Fluor® 647 anti-human CD11b Antibody (301319) and Alexa Fluor® 647 Mouse IgG1, κ Isotype Ctrl (FC) Antibody (400130) from Biolegend (San Diego, CA, USA). Propidium Iodide (P3566) from ThermoFisher Scientific (Waltham, MA, USA). Primers were from Integrated DNA Technologies (Coralville, IA, USA).

Animals

The zebrafish (*Danio rerio*) experiments were conducted in accordance with internationally accepted standards. The Animal Care and Use Protocols were approved by the Purdue Animal Care and Use Committee (PACUC), in accordance with the Guidelines for the Use of Zebrafish in the NIH Intramural Research Program (Protocol number: 1401001018).

Transient neutrophil-specific knockout zebrafish were generated by injecting Tol2 backbone plasmids into *LyzC*-Cas9-expressing embryos at their one-cell stage. Plasmids for transient

neutrophil-specific knockout of different genes were constructed using the following primers:

lats1 guide1 F:

GGAGGGCCGAGAAACCCGAGTTTAAGAGCTATGCTGGAAACAGCATAGC

lats1 guide1 R: CCTGGAAGTTTATCCTGTTTGAAGTAGGAGCCTGGAGAACTGC

lats1 guide2 F: GGATAAACTTCCAGGGTTTAAGAGCTATGCTGGAAACAGCATAGC

lats1 guide2 R: GTTCTCGGCCCTCCCGAACCAAGAGCTGGAGGGAGAGGCTGTAT

gcat guide1 F:

GGTGTTTTACAGCCAGCAGTTTAAGAGCTATGCTGGAAACAGCATAGC

gcat guide1 R: CGGCGCGGATAGAGTCCAGCGAACTAGGAGCCTGGAGAACTGC

gcat guide2 F: ACTCTATCCGCGCCGGTTTAAGAGCTATGCTGGAAACAGCATAGC

gcat guide2 R: GGGCTGTAAAACACCCGAACCAAGAGCTGGAGGGAGAGGCTGTAT

rabep1-1 guide1 F:

GAGCTGTCCGGGCGGCCAGGTTTAAGAGCTATGCTGGAAACAGCATAGC

rabep1-1 guide1 R: ATACAGCTTACCTGCCCCCGAACTAGGAGCCTGGAGAACTGC

rabep1-1 guide2 F:

GCAGGTAAGCTGTATGTTTAAGAGCTATGCTGGAAACAGCATAGC

rabep1-1 guide2 R:

CCGCCGGACAGCTCCGAACCAAGAGCTGGAGGGAGAGGCTGTAT

rabep1-2 guide1 F:

CCAACCGGTATCCAGATGGGTTTAAGAGCTATGCTGGAAACAGCATAGC

rabep1-2 guide1 R: TCCGAAGACCATCCTTATACGAACTAGGAGCCTGGAGAACTGC

rabep1-2 guide2 F:

AGGATGGTCTTTCGGAGTTTAAGAGCTATGCTGGAAACAGCATAGC

rabep1-2 guide2 R: CTGGATAACCGTTGGCGAACCAAGAGCTGGAGGGAGA

arhgap20 guide1 F:

GAAGTTACATTGGAGGTCGGTTTAAGAGCTATGCTGGAAACAGCATAGC

arhgap20 guide1 R: TGCGTCAGCCTCGATCCCTCGAACTAGGAGCCTGGAGAACTGC

arhgap20 guide2 F:

ATCGAGGCTGACGCAGTTTAAGAGCTATGCTGGAAACAGCATAGC

arhgap20 guide2 R:

CTCCAATGTAACCTCCGAACCAAGAGCTGGAGGGAGAGGCTGTAT

vamp8 guide1 F:

GCACGAGCGACCTTCTGGGGTTTAAGAGCTATGCTGGAAACAGCATAGC

vamp8 guide1 R: CGGGCCAGAATTCGATCAACGAACTAGGAGCCTGGAGAAGCTGC

vamp8 guide2 F: TCGAATTCTGGCCCGGTTTAAGAGCTATGCTGGAAACAGCATAGC

vamp8 guide2 R: GAAGGTCGCTCGTGCCGAACCAAGAGCTGGAGGGAGA

praf2 guide1 F:

AGTAATCCGACGATTCCGGGTTTAAGAGCTATGCTGGAAACAGCATAGC

praf2 guide1 R: ATGGGCCTTGTACTGGAAGCGAACTAGGAGCCTGGAGAAGCTGC

praf2 guide2 F: CAGTACAAGGCCCATGTTTAAGAGCTATGCTGGAAACAGCATAGC

praf2 guide2 R: AATCGTCGGATTACTCGAACTAGGAGCCTGGAGAAGCTGC

Transgenic zebrafish lines were generated by co-injecting Tol2 backbone plasmids with Tol2 transposase mRNA into wild-type AB embryos at their one-cell stage.

Plasmids for *miR-190* overexpression were constructed using the following primers:

miR-190a F: CTGGCAGTACGGGCTGCCTCTCCTCCTACCCAT

miR-190a R: TAACAGCAGTTGGCTCAAGCACAGTGGGCCTAAGA

Plasmids for neutrophil-specific knockout of *rabep1* were constructed using the following primers:

rabep1-1 guide1 F:

GAGCTGTCCGGGCGGCCAGGTTTAAGAGCTATGCTGGAAACAGCATAGC

rabep1-1 guide1 R: ATACAGCTTACCTGCCCCCGAACTAGGAGCCTGGAGAAGCTGC

rabep1-1 guide2 F:

GCAGGTAAGCTGTATGTTTAAGAGCTATGCTGGAAACAGCATAGC

rabep1-1 guide2 R:

CCGCCCGACAGCTCCGAACCAAGAGCTGGAGGGAGAGGCTGTAT

Plasmids for *RABEP1* rescue were constructed using the following primers:

RFP-CAAX linearization F:

CTAACATGCGGTGACGTGGAGGAGAATCCCGGCCCTATGGTGTCTAAGGGCGAAGAGCTG

RFP-CAAX linearization R: GGTGGCGAGGTACCTGTATCACTG

RABEP1 linearization F: AGGTACCTCGCCACCATGGCGCAGCCGGGC

RABEP1 linearization R:

GTCACCGCATGTTAGAAGACTTCCTCTGCCCTCTGTCTCAGGAAGCTGGTTAATGT
CTGT

RABEP1 5-2 F: AGGCCTCAAAGATCAGGAGGATGATGAACAAC

RABEP1 5-2 R: GATCTTTTGAGGCCTCCAGCTCTTTAATTTTG

Cell Culture

HEK293T (CRL-11268) and HL-60 (CCL-240) were from the American Type Culture Collection (ATCC, Manassas, VA, USA). All cells were maintained at 37°C with 5% CO₂ in a Forma™ Steri-Cycle™ i160 CO₂ Incubator (NC1207547, ThermoFisher Scientific). HL-60 cells were cultured in RPMI-1640 supplemented with 10% FBS, 25 mM HEPES, 1% penicillin-streptomycin, 1% sodium bicarbonate, 1% sodium pyruvate, and 1% GlutaMax. HEK293T cells were cultured in DMEM supplemented with 10% FBS and 1% sodium bicarbonate. HL-60 cells were differentiated with 1.3% DMSO for 6 days. Cells were checked monthly for Mycoplasma using the ATCC Universal Mycoplasma Detection Kit.

To generate *RABEP1* knockdown HL-60 cell lines pLKO.5 lentiviral constructs with shRNA (*RABEP1* shRNA 1: TRCN0000327713, *RABEP1* shRNA 2: TRCN0000363576, *RABEP1* shRNA 3: TRCN0000369958) were used, and MISSION® TRC2 pLKO.5-puro Non-Mammalian shRNA Control Plasmid DNA was used as a non-targeting control.

The *RABEP1* rescue lentiviral constructs were generated by replacing TurboGFP of the *RABEP1* shRNA 3 inserted into MISSION® pLKO.1-puro-CMV-TurboGFP™ Positive Control Plasmid DNA backbone with shRNA resistant full-length *RABEP1* or 5-2 truncated *RABEP1* using the following primers:

shRNA – turboGFP linearization F: AATTCTCGACCTCGAGACAAATGGC

shRNA – turboGFP linearization R: GGTGGCGACCGGGAGCGC

Rabep1 insert linearization F: CTCCCGGTCGCCACCATGGCGCAGCCGGGCCCCG

Rabep1 insert linearization R: TCGAGGTTCGAGAATTTTCAGGAGAGCACACACTTGC

shRNA 369958 loop swap F:

CATTACTCGAGTAATGATTCAGTTCTTTAACCTTTTTGAATTCAGTTATTAATAGT

shRNA 369958 loop swap R:

ATTACTCGAGTAATGATTCAGTTCTTTAACCCCGGTGTTTCGTCCTTTCCA

shRNA 369958 resistant F:

TAAAGGAGCTTAACCACTATCTGGAAGCTGAGAAATCTTGT

shRNA 369958 resistant R: GGTAAAGCTCCTTTACCTTTGAGGCCTCCAGCTCT

Lentiviral constructs containing pCMV-dR8.2 dvpr and pCMV-VSV-G were co-transfected into HEK293T cells using the Lipofectamine 3000 transfection kit to produce lentivirus. The viral supernatant was collected at 48 and 72 hours post-transfection and then concentrated using a Lenti-X concentrator. HL-60 cells were spin-infected (2500g, 1.5 hours) with 3 ml of complete RPMI-1640 medium containing concentrated lentivirus supplemented with 4 µg/ml polybrene. The infected HL-60 cells were then selected with 2 µg/ml puromycin to establish stable cell lines.

RNA Sequencing

RNA sequencing was conducted as previously described. Briefly, whole kidney marrows from *Tg(LyzC-miR-190-dendra2)^{pu38}* and *Tg(LyzC-vector-dendra2)^{pu7}* were collected and processed into single-cell suspensions. Neutrophils were isolated and sorted using fluorescence-activated cell sorting (FACS). Total RNA was extracted and sent for sequencing at The Center for Medical Genomics at Indiana University School of Medicine. The samples were polyA-enriched and sequenced with Illumina HiSeq 4000 in ultra-low mode, yielding reads ranging from 37 Million to 44 million. The RNA-seq reads were aligned to the zebrafish reference genome (GRCz11) using STAR (v2.5) with the parameter: “-outSAMmapqUnique 60”.²⁷ Uniquely mapped reads were assigned to genes with featureCounts (from subread v1.5.1) using the parameters: “-p -Q 10” 28 Genes were filtered based on counts per million, fold-change, miR-190 target score, and p-values for further analysis. Finally, zebrafish genes lacking human orthologues were excluded.

Microinjection

Microinjections into fish embryos involved injecting 1 nl of a mixture containing 25 ng/µl plasmid, with or without 35 ng/µl Tol2 transposase mRNA, into the cytoplasm at the one-cell stage, depending on whether the goal was transient or transgenic.

Tailfin Wounding

Tailfin wounding was performed on 3 days post fertilization (dpf) zebrafish larvae, where the tailfin was cut as close to the notochord as possible and incubated at 28 °C for 1 hour. After incubation, the larvae were fixed with 4% paraformaldehyde for 2 to 24 hours in preparation for Sudan Black staining.

LTB4 Bathing

LTB4 chemoattractant bathing was performed on 3 dpf zebrafish larvae, where the larvae were exposed to 30 nM LTB4 at 28 °C for 15 minutes. After incubation, the larvae were fixed with 4% paraformaldehyde for 2 to 24 hours in preparation for Sudan Black staining.

Whole Body Neutrophil Counting

Whole-body neutrophil counting was performed on 3 dpf zebrafish larvae, which were either imaged under an AXIO Zoom V16 microscope (Zeiss, Thornwood, NY, USA) for GFP signal or fixed with 4% paraformaldehyde for 2 to 24 hours in preparation for Sudan Black staining.

Sudan Black Staining

Sudan Black staining was used to stain neutrophils after larval fixation. The staining was performed for 30 minutes in 0.024% Sudan Black, 0.1% Pheno in 70% EtOH, and then washed with 70% EtOH. The stained larvae were rehydrated with PBST (0.1% Tween-20) and subjected to pigment clearing by soaking in 1% KOH and 1% H₂O₂ at room temperature for 10 minutes. After depigmentation, the samples were washed three times with PBS and stored at 4°C for future analysis.

Neutrophil Motility Assay

Neutrophil motility assay was performed on 3-dpf zebrafish larvae, which were anesthetized with tricaine methanesulfonate and embedded in 1.5% low-melt agarose. The larvae were then placed into an Ibidi μ -Slide 8 Well High ibiTreat and immediately settled at the bottom. Neutrophil migration in the larvae's head was recorded using a Lionheart FX Automated Microscope (BioTek, Winooski, VT, USA) with a 10 \times phase objective at 28 °C for 30 minutes, capturing images every minute. Representative time-lapse fluorescence images of neutrophil motility were obtained using an LSM 710 laser scanning confocal microscope (Zeiss, Thornwood, NY, USA) with a 20 \times objective at 28 °C for 30 minutes with a 1-minute interval. Neutrophil movement was tracked using the ImageJ plugin MTrackJ.

Common Cardinal Vein Bacterial Infection Assay

Either mCherry- or GFP-expressing *Pseudomonas aeruginosa* (*P. aeruginosa*) strain PA01 was used. *P. aeruginosa* was grown on Vogel-Bonner Minimal (VBM) media with carbenicillin. A streak plate was prepared from frozen stock and incubated at 37 °C overnight. A fresh colony was selected and grown in 3 ml of Luria-Bertani (LB) media with 3 μ l of carbenicillin overnight at 37 °C until the stationary phase. The next day, the bacteria were subcultured for 2.5 hours in fresh LB to reach the mid-logarithmic phase (OD₆₀₀ ~ 0.3). Bacteria were washed three times in sterile PBS and resuspended in 1 ml of PBS. Larvae at 2 dpf were injected with approximately 1500 CFUs of *P. aeruginosa* into the common cardinal vein and incubated individually at 28°C in 96-well plates. Survival was monitored for four days.

Western Blotting

dHL-60 cells were collected by centrifugation at 250 x g at 4°C for 5 minutes, then washed once with dPBS. Cells were resuspended in 2x protease inhibitor in RIPA buffer for lysis and incubated on ice for 20 minutes. Lysed cells were centrifuged at maximum speed, and the supernatant was transferred to a new tube. 10 μ l of protein sample was added to 1 ml of Precision Red Advanced Protein Assay solution, mixed by inverting 10 times, and incubated at room temperature for 1 minute. The mixture was transferred to a cuvette, and OD was measured using a BioPhotometer (Eppendorf, Hamburg, Germany), with 10 \times OD readings calculated as the amount of protein (μ g/ μ l). 20 μ g of protein was mixed with RIPA buffer to a total volume of 20 μ l for each sample, then boiled at 95°C for 15 minutes after adding 4 μ l of 6 \times SDS dye. Samples were cooled on ice and centrifuged at maximum speed for 1 minute before loading onto a 10% polyacrylamide gel. All 24 μ l of each sample was loaded into individual wells, with PageRuler™ Prestained Protein Ladder used as a size marker. The

gel was first run at 90V for 30 minutes, then at 140V for 1 hour in Novex™ Tris-Glycine SDS Running Buffer. After electrophoresis, the gel was trimmed to remove the stacking gel and assembled in a gel holder cassette in the order: sponge, paper, gel, PVDF transfer membrane, paper, sponge. The transfer was performed at 60V for 1.5 hours in Pierce™ 10X Western Blot Transfer Buffer. After transfer, the PVDF membrane was cut to match the size of the gel and blocked with 2.5% milk in PBST at room temperature for 1 hour. The membrane was probed overnight at 4°C on a shaker with primary antibodies diluted 1:1000 in 1% BSA in PBST. After washing three times with PBST at 5-minute intervals, it was probed with secondary antibodies diluted 1:5000 in 1% BSA in PBST at room temperature for 30 minutes in the dark. The membrane was washed three additional times with PBST and then imaged using an LI-COR Odyssey Gel Imaging Scanner (BioAgilytix, Durham, NC, USA). For the phospho-PAK western blot, cells were first counted and adjusted to 5×10^6 cells/ml, then starved in serum-free RPMI-1640 medium for 1 hour. Cells were aliquoted into six time points: 0 sec, 30 sec, 1 min, 2 min, 5 min, and 10 min, each stimulated with 100 nM final concentration of fMLP. Stimulation was halted by adding an equal volume of ice-cold stop solution (20% TCA, 40 mM NaF, and 20 mM β -glycerophosphate), and then the sample was kept on ice for 1 hour for lysis. Lysates were pelleted at $14,000 \times g$ for 10 minutes, washed once with 1 ml of ice-cold 0.5% TCA, and resuspended in 2 \times Laemmli sample buffer. After preparation, a phospho-PAK western blot was performed as described above.

Rab5-GTP Pull-Down

A Rab5 Pull-Down Activation Assay Kit (NewEast Biosciences) was used to isolate active Rab5 from whole-cell lysate by affinity precipitation. dHL-60 cells were counted and resuspended in ice-cold lysis buffer at a concentration of 10^7 cells/ml. Cells were then lysed by pipetting and centrifuged at $12,000 \times g$ at 4°C for 10 minutes. The supernatant was collected for immediate use. The cell lysate was divided into two tubes: one for measuring Rab5 protein levels and the other for affinity precipitation of active Rab5. For affinity precipitation, 1 μ l of anti-Rab5-GTP antibody and 20 μ l of resuspended bead slurry were added. The mixture was incubated at 4°C for 1 hour. The beads were then centrifuged at $5,000 \times g$ for 1 minute. Pelleted beads were washed three times with lysis buffer, resuspended in 2 \times Laemmli sample buffer, and boiled at 95°C for 5 minutes. The prepared samples were centrifuged at $5,000 \times g$ for 10 seconds before immunoblotting. Fifteen microliters of pull-down supernatant and 15 microliters of cell lysate were used for Western blotting. Anti-Rab5 rabbit polyclonal antibody, diluted 1:500 in 3% BSA in TBST, was used as the primary antibody. Goat anti-rabbit IgG (H+L) secondary antibody (DyLight™ 800 4X PEG) diluted 1:1000 in 3% BSA in TBST was used as the secondary antibody.

Under-Agarose Random Migration Assay

Ibidi μ -Slide 8 Well High ibiTreat or μ -Slide 8 Well High Glass Bottom slides were first coated by adding 500 μ l of fibrinogen at a concentration of 100 nM and incubated for 1 hour at 37°C. Residual fibrinogen solution was aspirated, and the slides were washed once with dPBS, then blocked with 2% BSA in dPBS at 37°C for 30 minutes. Slides were washed again with dPBS and left to air-dry overnight in the cell culture hood without UV exposure. dHL-60 cells were collected and resuspended in mHBSS at 5×10^5 cells/mL. Then, 5 μ l

of this cell suspension was added to the center of each well of the fibrinogen-coated slides, and the wells were topped with 500 μ l of 1.5% Low Melt Agarose in mHBSS with 100 nM fMLP. The slides were centrifuged at 2000 x g and 25°C for 5 minutes to allow cells to settle under the agarose gel. Imaging was performed using a Lionheart FX Automated Microscope (Biotek, Winooski, VT, USA) with a 10 \times phase objective at 37°C for 2 hours, with images taken at 1-minute intervals. dHL-60 cell movement was tracked using the ImageJ plugin MTrackJ.

Flow Cytometry Analysis

dHL-60 cells were collected and resuspended in 100 μ l mHBSS at a concentration of 1×10^6 cells/ml. Cells were stained with BD Horizon™ BV421 Annexin V, Alexa Fluor® 647 anti-human CD11b Antibody, and Propidium Iodide. Another aliquot of cells at the same concentration was stained with anti-Mouse IgM, κ Isotype Control, Alexa Fluor® 647 Mouse IgG1, κ Isotype Ctrl (FC) Antibody, and Propidium Iodide as the control group. All samples were incubated on ice for 30 min, centrifuged at 300 x g at 4°C for 5 min, then washed with eBioscience™ Flow Cytometry (FACS) Staining Buffer. Cells were centrifuged under the same parameters, then resuspended in 350 μ L of FACS Staining Buffer and placed back on ice for flow cytometry analysis. Flow cytometry was performed using LSR Fortessa™ X-20 Cell Analyzer (BD Biosciences, Franklin Lakes, NJ, USA).

Phagocytosis Assay

pHrodo™ Green E. coli BioParticles™ Conjugates (Invitrogen) were reconstituted in mHBSS and sonicated at 10% amplitude for 5 min with 10-sec intervals. 5×10^5 dHL-60 cells were resuspended in 100 μ l of BioParticle suspension and incubated at 37°C for 1 hr. Phagocytosis activity was stopped by placing the cells on ice, and 250 μ L of mHBSS was added to increase the total volume for flow cytometry analysis. A total number of 5×10^5 dHL-60 cells in 350 μ l mHBSS was used as a control. Flow cytometry was performed using an LSR Fortessa X-20 Cell Analyzer (BD Biosciences, Franklin Lakes, NJ, USA). Data were analyzed using FlowJo (BD Biosciences) to quantify the geometric mean FITC intensity.

Reactive Oxygen Species Assay

The Amplex Red Hydrogen Peroxide Peroxidase Assay Kit (Invitrogen) was used to detect ROS production after PMA stimulation. dHL-60 cells were collected and resuspended in 1 mL of Krebs-Ringer phosphate (KRPG) solution at a concentration of 7.5×10^5 cells/mL. The KRPG solution contains 145 mM NaCl, 5.7 mM sodium phosphate, 4.86 mM KCl, 0.54 mM CaCl₂, 1.22 mM MgSO₄, and 5.5 mM glucose, with a pH of 7.35. Twenty microliters of cell suspension were added to each well of a black-walled 96-well plate, along with 20 microliters of prepared H₂O₂ standards at concentrations of 0 to 90 μ M. The reaction mix was prepared by combining 60 μ L of 50 μ M Amplex Red with 120 μ L of 10 U/mL horseradish peroxidase (HRP) in 12 mL of KRPG solution. The reaction mixture was then modified to include 0.5 ng/ μ L phorbol 12-myristate 13-acetate (PMA) or, as a control, an equal volume of DMSO. One hundred microliters of the modified reaction mix were added to the cells for three technical replicates, while 100 μ L of the unmodified reaction mix was added to H₂O₂ standards to achieve final concentrations of 0–15 μ M. ROS readings were

taken every 15 minutes over 45 minutes immediately after stimulation, using a Synergy Neo2 (BioTek) with an excitation/emission wavelength of 490/550 nm. Each reading was corrected by subtracting the average background fluorescence measured in each condition. The adjusted fluorescence intensity was then plotted against the standard curve to determine the amount of ROS produced at each time point and condition. The difference between the PMA condition and the DMSO control was considered the actual ROS produced, since PMA is dissolved in DMSO, and this method accounts for the background in the PMA condition. All readings were normalized to the amount of ROS produced by the control at each time point. The final analysis quantified total ROS production over the 45 minutes, normalized to the control.

Immunofluorescence Staining

dHL-60 cells were resuspended in mHBSS at a concentration of 1×10^6 cells/ml and attached to fibrinogen-coated slides for 30 minutes. Cells were stimulated with 100 nM fMLP for 30 minutes and fixed with 4% paraformaldehyde in dPBS for 15 minutes at 37°C. They were then permeabilized in PBS with 0.1% Triton X-100 at room temperature for 1 hour. Permeabilized cells were incubated with Alexa Fluor™ 488 Phalloidin and Phospho-Myosin Light Chain 2 diluted to 1:100 in 3% BSA at 4°C overnight, depending on the staining purpose. The cells were stained with secondary antibodies diluted to 1:500 in 3% BSA and DAPI at room temperature for 1 hour. Finally, stained cells were imaged for fluorescence using a Zeiss LSM 880 Confocal Laser Scanning Microscope (Zeiss, Thornwood, NY, USA) with a 63× oil immersion objective lens.

Wheat Germ Agglutinin and Transferrin Endocytosis Dynamics

dHL-60 cells were resuspended in RPMI-1640 medium at a concentration of 5×10^5 cells/mL. The cells were then incubated at 37°C with a final concentration of 100 nM fMLP, 25 µg/mL of transferrin (Tfn), and 5 µg/mL of WGA. Cells were fixed at 0, 5, and 10 minutes after incubation to determine the internalization rate of the Tfn and WGA. Afterward, the cells were washed once with RPMI-1640 medium, resuspended in RPMI-1640 medium containing 100 nM fMLP, and fixed at 0, 5, 10, and 15 minutes after washing to determine the recycling rate of Tfn receptor and WGA. Fixed cells were mounted on Ibidi µ-Slide 8 Well High ibi-Treat with 200 µL of VECTASHIELD HardSet Antifade Mounting Medium. Imaging was performed using a Zeiss LSM 900 Confocal Laser Scanning Microscope (Zeiss, Thornwood, NY, USA) with a 20× objective lens.

Statistical Analysis

Statistical analysis was performed with Prism 6 (GraphPad), where the Mann-Whitney test was used to compare the two groups. Dunnett's multiple comparisons test was used to compare more than three groups to determine statistical significance. Individual p-values are indicated in the figures. Each statistical analysis was done on all biological repeats, with different repeats indicated with varying shades of color in the resulting graphs.

Results

Overexpression of *miR-190* in zebrafish neutrophils suppresses neutrophil random migration and chemotaxis.

Our previous study found that overexpression (OE) of miR-190s in zebrafish neutrophils reduces their recruitment to an ear infection or tail wound site.²¹ To verify these findings, we thoroughly characterized the transgenic lines *Tg(LyzC-miR-190-dendra2)^{pu38}* and *Tg(LyzC-vector-dendra2)^{pu7}*, which express miR-190 from the spliced intron or the Dendra2 vector control (Fig. 1A). We performed tailfin transection to assess neutrophil recruitment to a wound (Fig. 1B). The average number of neutrophils migrating to the wound within the first hour is significantly lower in miR-190 OE zebrafish compared to controls (Fig. 1C-D). After validation, we used LTB₄ as a chemoattractant to recruit neutrophils from the caudal hematopoietic tissue (CHT) to the caudal fin (Fig. 1E). The percentage of neutrophils that migrated out was notably reduced in miR-190 OE fish compared to controls (Fig. 1F, G). Live imaging of the zebrafish head mesenchyme was performed to observe neutrophil motility, where neutrophils move spontaneously (Fig. 1H, Supplemental Video 1). miR-190 OE neutrophils showed a significantly decreased speed compared to controls (Fig. 1I). Lastly, to exclude the possibility that miR-190 OE affects neutrophil development or survival, total neutrophil counts were performed, which showed no difference between control and OE fish (Fig. 1J, K). All experiments were conducted on offspring from two different miR-190 OE founders to avoid artifacts related to random transgene insertion sites (Supplemental Fig. 1, Supplemental Video 2). In summary, miR-190 suppresses neutrophil motility and chemotaxis across all tested conditions. Additionally, we infected 2 dpf miR-190 OE larvae with GFP- or RFP-labeled *Pseudomonas aeruginosa* (*P. aeruginosa*) via common cardinal vein injections (Fig. 1L). Monitoring survival up to 4 days post-infection (dpi) revealed that miR-190 OE larvae have significantly lower survival rates than controls, suggesting immune deficiency (Fig. 1M).

A neutrophil-specific knockout screen identifies *rabep1* as a potential regulator for neutrophil migration in zebrafish.

To understand how miR-190 regulates neutrophil migration, we sorted neutrophils from whole kidney marrow, performed RNA sequencing, and identified differentially expressed genes (DEGs) upon miR-190 OE (Fig. 2A). GO enrichment analysis revealed that the downregulated DEGs are involved in biological processes such as estrogen-dependent gene expression, chromatin organization, Rho GTPase effectors, and Rho GTPase signaling pathways (Fig. 2B). To find the direct targets of miR-190, we further filtered the DEGs with a miR-190 target score (<-0.25), p-value (<0.13), and fold change ($\log_2\text{FC} < -1.5$), resulting in a list of six potential direct targets of miR-190 (Fig. 2A; Table 1). We then used the CRISPR-Cas9 system to transiently knock out each gene specifically in neutrophils²² to determine their roles in neutrophil migration. Injecting a plasmid expressing neutrophil-specific sgRNAs and GFP into the neutrophil-specific Cas9-expressing line with an eye marker (*Tg(LyzC: Cas9, Cry: GFP/RFP)^{pu34/pu52}*) allowed us to track neutrophil motility without creating stable lines (Fig. 2C). Knockout of *praf2* or *rabep1* resulted in a significant decrease in neutrophil speed (Fig. 2D). To rule out possible off-target effects of *rabep1*-1

sgRNA, we used a different sgRNA (*rabep1-2*) to knockout *rabep1* and observed the same phenotype, confirming that *rabep1* is necessary for neutrophil motility.

***Rabep1* is essential for neutrophil migration and chemotaxis in zebrafish.**

To further confirm the results of our transient screen, we created lines with a neutrophil-specific knockout of *rabep1* (Fig. 3A). Similar to miR-190 OE, *rabep1* knockout led to reduced neutrophil recruitment to a wound site (Fig. 3B, C), impaired LTB4-induced mobilization (Fig. 3D, E), decreased motility in the head mesenchyme (Fig. 3F, G, Supplemental Video 3), without affecting overall neutrophil numbers (Fig. 3H, I). Additionally, we infected *rabep1* knockout larvae at 2 dpf with either GFP- or RFP-labeled *P. aeruginosa*. We observed that *rabep1* knockout fish had significantly lower survival rates compared to controls, indicating a diminished ability to clear bacteria (Fig. 3J). The *Rabep1* gene encodes the Rabaptin-5 protein, which acts as an effector of the small GTPases Rab4 and Rab5, facilitating membrane recycling or endosomal maturation of early endosomes.²³⁻²⁶ The human *RABEP1* gene and the zebrafish *rabep1* gene are highly conserved, sharing 70.94% homology. Rabaptin-5 contains multiple Rab4- and Rab5-binding domains that interact with active Rab4 or Rab5, as well as a Rabex-5 binding site, which promotes Rab5 activation.²⁹⁻³⁰ A previous study identified the functional domains of Rabaptin-5 by rescuing its knockdown with various truncations. A truncation lacking a Rab5-binding domain and part of a Rab4-binding domain (5-2 RABEP1) showed the most pronounced phenotype, characterized by large, malformed endosome structures.²⁴ Using a similar approach, we generated *Tg(LyzC:FL RABEP1-RFP-CAAX)^{pu53}* and *Tg(LyzC: 5-2 RABEP1-RFP-CAAX)^{pu54}* lines and crossed them with *rabep1* TSKO fish. As a control, we crossed *rabep1* TSKO with *Tg(LyzC: RFP-CAAX)^{pu54}*. Expression of full-length *RABEP1*, but not 5-2 *RABEP1*, rescued the *rabep1* TSKO phenotype (Fig. 3K-M, Supplemental Video 4).

***RABEP1* is essential for the migration of dHL-60 cells.**

HL-60 cells differentiate into neutrophil-like cells, exhibiting features such as migration, chemotaxis, ROS production, and phagocytosis.³¹ We generated stable *RABEP1* knockdown cell lines using lentiviral transduction with three different shRNAs and confirmed the knockdown (Fig. 4A, B). A cell line with a non-targeting control shRNA served as a control. In subsequent experiments, we concentrated on the two cell lines with higher knockdown efficiency (shRNA2 and shRNA3). To determine whether RABAPTIN affects cell differentiation, we performed flow cytometry analysis to measure surface expression of CD11b, a maturation marker. *RABEP1* shRNA2 and shRNA3 lines showed over 50% and 90% CD11b-positive populations, respectively. The cell populations appeared healthy, with low apoptosis levels (Supplemental Fig. 2A). Next, we conducted under-agarose random migration assays on fibrinogen-coated slides to track the movement of dHL-60 cells. Both *RABEP1* knockdown lines exhibited a significant reduction in migration speed compared to the control (Fig. 4C, D; Supplemental Video 5). To explore whether RABAPTIN plays a role in other neutrophil functions, we measured phagocytosis and ROS production. The rates of phagocytosis and ROS production in *RABEP1* knockdown cells were similar to those of the control (Supplemental Fig. 2B-E), suggesting that RABAPTIN is particularly important for cell motility.

We then performed a rescue experiment similar to the zebrafish model, stably expressing the TurboGFP control, FL, or 5-2 RABAPTIN in the shRNA3 line. Control shRNA cell lines expressing TurboGFP were generated for comparison. Western blot analysis confirmed knockdown of *RABEP1* and overexpression of both FL and 5-2 RABAPTIN (Fig. 4E, F). All lines were similarly differentiated and viable (Supplemental Fig. 2F). Consistent with the zebrafish findings, only FL RABAPTIN expression restored the under-agarose migration defect in *RABEP1* knockdown cells (Fig. 4G, H, Supplemental Video 6).

***RABEP1* regulates endosomal recycling, cell signaling, and actin polymerization.**

The known function of Rabaptin relates to early endosome recycling and maturation into late endosomes, where we speculate that fast recycling to the plasma membrane via Rab4-GTP recruitment drives downstream signaling pathways, such as Rac activation for actin polymerization, which are essential for precise neutrophil migration (Fig. 5A). To investigate membrane trafficking, we first incubated the cells with wheat germ agglutinin (WGA) and Transferrin (Tfn) to label total membrane and fast recycling endosomes.³² Cells were fixed at 0, 5, and 10 minutes after incubation to determine the internalization dynamics, which were comparable between the control and the *RABEP1* knockdown group (Fig. 5B-D). Next, cells were allowed to uptake WGA and Tfn for 30 minutes, then washed and resuspended in media free of WGA and Tf ligands. Cells were fixed at 0, 5, 10, and 15 minutes after washing to assess recycling dynamics (Fig. 5E). While control cells rapidly recycled Tfn receptors, *RABEP1* knockdown cells showed a significantly slower recycling rate (Fig. 5F). Additionally, WGA was retained in *RABEP1* knockdown cells (Fig. 5G). We also investigated whether this accumulation resulted from reduced Rab5 activation due to the failure of recruiting Rabex5, the Rab5 GEF. Using a Rab5-GTP pull-down assay to measure active Rab5 directly, we did not observe any significant difference in Rab5 activity between these cell lines (Supplemental Fig. 3).

It has been shown that endosomal signaling is essential for activating Rac1, the Ras-related C3 botulinum toxin substrate 1.³³ Specifically, chemokine-stimulated CCR7 internalization through endocytosis is crucial for Rac1 activation. The activation of PAK into phosphorylated PAK (pPAK) by Rac and Cdc42 GTPases is vital in neutrophil migration, where downstream signals of pPAK, such as phosphorylation of myosin light chain (MLC) or activation of actin-binding proteins, are necessary for cell movement.³⁴⁻³⁷ To determine whether reduced motility in *RABEP1* knockdown cell lines relates to this pathway, we measured PAK activation by assessing its phosphorylation via western blot. Indeed, PAK activation, indicated by the pPAK/PAK ratio, is significantly decreased in both knockdown cell lines at various time points after fMLP stimulation (Fig. 5H, I). We then examined whether the cells could polarize to understand the motility defect in Rabaptin-5-deficient cells. All cell lines exhibited polarized F-actin and myosin light chain (MLC) distribution after fMLP stimulation, indicating that cell polarization is independent of Rabaptin-5 (Fig. 5J, K).³⁸⁻³⁹ However, the total F-actin content was lower in Rabaptin-5-deficient cells, consistent with Rac's role in driving branched actin polymerization at the lamellipodia at the cell front (Fig. 5L, M).

To further elucidate the role of Rab4 and Rab5 in neutrophil migration, we transiently overexpressed dominant negative (DN) Rab4 (S27N) or Rab5 (S34N) in zebrafish neutrophils. Again, both Rab4 DN and Rab5 DN OE neutrophils showed a phenocopy of *rabep1* TSKO neutrophils (Supplemental Fig. 4; Supplemental Video 7), suggesting the importance of the endocytic recycling pathway in neutrophil motility.

Discussion

Here, we report that the miR-190 target gene *Rabep1* is crucial for the migration of zebrafish neutrophils and dHL-60 cells. RABAPTIN regulates the rapid recycling of early endosomes, facilitating the activation of the pPAK pathway and sustained F-actin polymerization, which is required for locomotion. Overall, we have uncovered a mechanism by which *RABEP1* regulates neutrophil motility. While dHL-60 cells are a suitable model for studying the genetic regulation of chemotaxis⁴⁰⁻⁴¹, validating the observation in Hoxb8 or iPS cell-derived neutrophils can further validate this conclusion in future studies. Another limitation of the work is the lack of specificity regarding the cargos that are rapidly recycled to drive sustainable cell polarization.

MiR-190 has been linked to suppressing breast cancer metastasis, with metastatic breast cancer cells showing significantly lower levels of miR-190 expression compared to normal breast cells.⁴² In another cancer type, hepatocellular carcinoma, miR-190 promotes proliferation and metastasis by targeting a tumor suppressor.⁴³ Given the broad range of target genes for miR-190, it is being studied as a potential therapeutic target and biomarker in various diseases, especially cancer.⁴⁴⁻⁴⁵ Our initial screening of miR-190 target gene transient knockout in zebrafish neutrophils identified several genes that may influence cell migration, such as *praf2*, *lats1*, and *rabep1*. Whether these targets all have essential functions in cancer remains to be tested. Additionally, follow-up studies on other screened miR-190 target genes, *praf2* and *lats1*, may uncover new mechanisms that regulate cell migration.

Rabaptin is a scaffolding protein that mediates the recruitment of both Rab4-GTP and Rab5-GTP to early endosomes while also acting as an exchange factor of Rab5 through its binding with Rabex5.⁴⁶ Interestingly, it has been reported that Rab5-GTP binds with higher affinity to the C-terminus binding site of Rabaptin, whereas Rab4-GTP binds more effectively at the binding site that includes the coil-coiled (CC) 1-2 domain.²⁹ The 5-2 Rabaptin lacks a low-affinity binding site for Rab5 GTP and a high-affinity binding site for Rab4 GFP and cannot rescue the *rabep1* TSKO or *RABEP1* shRNA phenotype. We therefore speculate that Rabaptin recruitment of Rab4-GTP to early endosomes is essential for neutrophil migration. Moreover, Rab5 activation appears normal in *RABEP1* knockdown cells, suggesting that RABAPTIN is not necessary for RAB5 activation in dHL-60 cells. It has been shown that the Rabex5 GEF domain is constantly active but is autoinhibited by its CC domains.⁴⁷ The binding of Rabex5 to Rabaptin enables a conformational change that exposes the GEF domain and enhances GEF activity.⁴⁸ Conversely, others report that Rabex5 GEF activity can be activated independently of Rabaptin interaction, specifically through the Rabex5 early endosome targeting (EET) domain, which enables interaction with early endosomes that may relieve autoinhibition of the CCs.⁴⁹ Based on the similar phenotypes observed with Rab4/5 DN and *rabep1* knockout, our data suggest that Rabaptin binds to Rab5-GTP

on early endosomes and then recruits Rab4-GTP to promote early endosome recycling, a process critical for neutrophil migration.

Our results align with previous findings indicating that endocytosis is crucial for cell migration, although this had not been confirmed in neutrophils before this study. Loss of Sprint, another Rab5 GEF protein, causes severe migration defects in the border cells of *Drosophila* during oogenesis.⁵⁰ Restricting the activation of protein kinase C (PKC) α promotes Rab4-dependent recycling of the platelet-derived growth factor β receptor (PDGFR) in mouse embryonic fibroblasts, resulting in increased chemotaxis.⁵¹ Rabaptin is also identified as a substrate for protein kinase D (PKD), which regulates the formation of the Rab4-Rabaptin complex necessary for rapid recycling of $\alpha v \beta 3$ integrins; this process is essential for persistent cell motility and tumor cell invasion.⁵² Our study specifically highlights the role of Rab4/5-GTP in neutrophil migration by modulating Rac1 activation. Activation of Rac1 causes its translocation to the cell surface via recycling endosomes, a process reported to respond to stimulation of CCR7 and various receptor tyrosine kinases.⁵³⁻⁵⁴ From this subcellular location, Rac1 activates the main effector PAK1, which phosphorylates LIM kinase and cortactin, among others, to coordinate actin polymerization at the plasma membrane.⁵⁵ This polymerization results in the formation of cytoskeletal actin filaments that support the stability of new filopodia and lamellipodia. Since these membrane protrusions are a key step in cell migration, endosomal Rac1 activation plays a central role in this physiological process.⁵⁶

Although there have been a few reports on diseases related to mutations in *RABEP1*, such as increased breast cancer invasion with inhibition of *RABEP1* expression or decreased tumor cell migration when phosphorylation of RABAPTIN is disrupted, the role of *RABEP1* in leukocytes has not been established. Our findings that *RABEP1* is necessary for neutrophil migration may provide insights into the mechanisms behind leukocyte-related diseases, such as acute respiratory distress syndrome (ARDS), rheumatoid arthritis, or sepsis, and could serve as a potential target for therapeutic strategies.⁵⁷⁻⁶⁰

Supplementary Material

Refer to Web version on PubMed Central for supplementary material.

Acknowledgments and Sources Funding

We thank our undergraduate students, Caroline Powell and Loahni Hernandez, for cell tracking, counting, and maintaining our zebrafish lines. Special thanks to Hyein Park for the critical reading of the manuscript and intellectual feedback. We thank the Purdue Imaging Facility for assistance with data collection. The authors gratefully acknowledge the support of the Flow Cytometry and Cell Separation Facility from the Institute for Cancer Research, NIH grant P30 CA023168. This work is supported by NIH-R35GM119787 (to QD), NIH-R01CA293514 (to XB), and NIH-R37CA265926 (to XB).

Data Available

The RNA sequencing data can be accessed at <https://www.ncbi.nlm.nih.gov/geo/query/acc.cgi?acc=GSE167554>, GEO accession number GSE167554. Other data will be made available upon reasonable request.

References

1. Nathan C. 2006. Neutrophils and immunity: challenges and opportunities. *Nat Rev Immunol.* 6:173–182. doi:10.1038/nri1785. [PubMed: 16498448]
2. Sadik CD, Kim ND, Luster AD. 2011. Neutrophils cascading their way to inflammation. *Trends Immunol.* 32:452–460. doi:10.1016/j.it.2011.06.008. [PubMed: 21839682]
3. Nauseef WM, Borregaard N. 2014. Neutrophils at work. *Nat Immunol.* 15:602–611. doi:10.1038/ni.2921. [PubMed: 24940954]
4. Witko-Sarsat V, Rieu P, Descamps-Latscha B, Lesavre P, Halbwachs-Mecarelli L. 2000. Neutrophils: molecules, functions and pathophysiological aspects. *Lab Invest.* 80:617–653. doi:10.1038/labinvest.3780067. [PubMed: 10830774]
5. Segal AW. 2005. How neutrophils kill microbes. *Annu Rev Immunol.* 23:197–223. doi:10.1146/annurev.immunol.23.021704.115653. [PubMed: 15771570]
6. Fu X, Liu H, Huang G, Dai S. 2021. The emerging role of neutrophils in autoimmune-associated disorders: effector, predictor, and therapeutic targets. *MedComm.* 2:402–413. doi:10.1002/mco2.85. [PubMed: 34766153]
7. Németh T, Mócsai A, Lowell CA. 2016. Neutrophils in animal models of autoimmune disease. *Semin Immunol.* 28:174–186. doi:10.1016/j.smim.2016.03.003. [PubMed: 27067180]
8. Chou RC, Jiang D, Sheldon A, Segal LN, Besin G, et al. 2010. Lipid-cytokine-chemokine cascade drives neutrophil recruitment in a murine model of inflammatory arthritis. *Immunity.* 33:266–278. doi:10.1016/j.immuni.2010.07.004. [PubMed: 20727790]
9. Dinauer MC. 2003. Regulation of neutrophil function by Rac GTPases. *Curr Opin Hematol.* 10:8–15. doi:10.1097/00062752-200301000-00003. [PubMed: 12483106]
10. Downey GP, Dong Q, Kruger J, Dedhar S, Cherapanov V. 1999. Regulation of neutrophil activation in acute lung injury. *Chest.* 116:46S–54S. doi:10.1378/chest.116.suppl_1.46s.
11. Christopher MJ, Link DC. 2007. Regulation of neutrophil homeostasis. *Curr Opin Hematol.* 14:3–8. doi:10.1097/MOH.0b013e328011ef5f. [PubMed: 17133093]
12. Ward JR, Heath PR, Catto JW, Whyte MKB, Milo M, et al. 2011. Regulation of neutrophil senescence by microRNAs. *PLoS One.* 6:e15810. doi:10.1371/journal.pone.0015810. [PubMed: 21283524]
13. Friedman RC, Farh KK-H, Burge CB, Bartel DP. 2009. Most mammalian mRNAs are conserved targets of microRNAs. *Genome Res.* 19:92–105. doi:10.1101/gr.082701.108. [PubMed: 18955434]
14. Radom-Aizik S, Zaldivar F, Oliver S, Galassetti P, Cooper DM. 2010. Evidence for microRNA involvement in exercise-associated neutrophil gene expression changes. *J Appl Physiol.* 109:252–261. doi:10.1152/jappphysiol.00052.2010. [PubMed: 20110541]
15. Speier S, Nyqvist D, Cabrera O, Yu J, Molano RD, et al. 2008. Noninvasive high-resolution in vivo imaging of cell biology in the anterior chamber of the mouse eye. *Nat Protoc.* 3:1278–1286. doi:10.1038/nprot.2008.89. [PubMed: 18714296]
16. De La Rosa IA, Perez-Sanchez C, Ruiz-Limon P, Lopez-Pedreira C, Castro-Villegas MC, et al. 2020. Impaired microRNA processing in neutrophils from rheumatoid arthritis patients confers their pathogenic profile: modulation by biological therapies. *Haematologica.* 105:2250–2261. doi:10.3324/haematol.2019.230011. [PubMed: 33054050]
17. Lieschke GJ, Currie PD. 2007. Animal models of human disease: zebrafish swim into view. *Nat Rev Genet.* 8:353–367. doi:10.1038/nrg2091. [PubMed: 17440532]
18. Zhou W, Pal AS, Hsu AY, Gurol T, Zhu X, et al. 2018. MicroRNA-223 suppresses the canonical NF- κ B pathway in basal keratinocytes to dampen neutrophilic inflammation. *Cell Rep.* 22:1810–1823. doi:10.1016/j.celrep.2018.01.046. [PubMed: 29444433]
19. Sullivan C, Kim CH. 2008. Zebrafish as a model for infectious disease and immune function. *Fish Shellfish Immunol.* 25:341–350. doi:10.1016/j.fsi.2008.05.005. [PubMed: 18640057]
20. Fan HB, Liu XJ, Qiu XY, Zhang BH, Wan J, et al. 2014. miR-142-3p acts as an essential modulator of neutrophil development in zebrafish. *Blood.* 124:1320–1330. doi:10.1182/blood-2014-03-560839. [PubMed: 24990885]

21. Hsu AY, Wang J, Zhang W, Wang J, Zhou W, et al. 2019. Phenotypical microRNA screen reveals a noncanonical role of CDK2 in regulating neutrophil migration. *Proc Natl Acad Sci USA*. 116:18561–18570. doi:10.1073/pnas.1905221116. [PubMed: 31451657]
22. Wang Y, Zhang C, Xu Y, He Y, Ma H, et al. 2020. A robust and flexible CRISPR/Cas9-based system for neutrophil-specific gene editing in zebrafish. *J Cell Sci*. 133:jcs240879. doi:10.1242/jcs.240879. [PubMed: 32005702]
23. Horiuchi H, Lippe R, McBride HM, Rubino M, Woodman P, et al. 1997. A novel Rab5 GDP/GTP exchange factor complexed to Rabaptin-5 links nucleotide exchange to effector recruitment and function. *Cell*. 90:1149–1159. doi:10.1016/S0092-8674(00)80357-7. [PubMed: 9323142]
24. Kälin S, Hirschmann DT, Buser DP, Spiess M. 2015. Rabaptin5 is recruited to endosomes by Rab4 and Rabex5 to regulate endosome maturation. *J Cell Sci*. 128:3967–3980. doi:10.1242/jcs.174664.
25. Van Der Sluijs P, Hull M, Zahraoui A, Tavitian A, Goud B, et al. 1992. The small GTP-binding protein rab4 controls an early sorting event on the endocytic pathway. *Cell*. 70:729–740. doi:10.1016/0092-8674(92)80066-W. [PubMed: 1516131]
26. Mohrmann K, Gerez L, Oorschot V, Klumperman J, Van Der Sluijs P. 2002. Rab4 function in membrane recycling from early endosomes depends on a membrane to cytoplasm cycle. *J Biol Chem*. 277:32029–32035. doi:10.1074/jbc.M202470200. [PubMed: 12036958]
27. Dobin A, Davis CA, Schlesinger F, Drenkow J, Zaleski C, et al. 2013. STAR: ultrafast universal RNA-seq aligner. *Bioinformatics*. 29:15–21. doi:10.1093/bioinformatics/bts635. [PubMed: 23104886]
28. Liao Y, Smyth GK, Shi W. 2014. featureCounts: an efficient general purpose program for assigning sequence reads to genomic features. *Bioinformatics*. 30:923–930. doi:10.1093/bioinformatics/btt656. [PubMed: 24227677]
29. Vitale G, Rybin V, Christoforidis S, Thornqvist P, McCaffrey M, et al. 1998. Distinct Rab-binding domains mediate the interaction of Rabaptin-5 with GTP-bound rab4 and rab5. *EMBO J*. 17:1941–1951. doi:10.1093/emboj/17.7.1941. [PubMed: 9524117]
30. Stenmark H, Vitale G, Ullrich O, Zerial M. 1995. Rabaptin-5 is a direct effector of the small GTPase Rab5 in endocytic membrane fusion. *Cell*. 83:423–432. doi:10.1016/0092-8674(95)90144-5. [PubMed: 8521472]
31. Bhakta SB, Smith J, Brown K, Nguyen T, Lee R, et al. 2024. Neutrophil-like cells derived from the HL-60 cell line as a genetically-tractable model for neutrophil degranulation. *PLoS One*. 19:e0297758. doi:10.1371/journal.pone.0297758. [PubMed: 38324578]
32. Mayle KM, Le AM, Kamei DT. 2012. The intracellular trafficking pathway of transferrin. *Biochim Biophys Acta Gen Subj*. 1820:264–281. doi:10.1016/j.bbagen.2011.09.009.
33. Hahn H, Peters A, Kumar S, Li F, Jones K, et al. 2025. Endosomal chemokine receptor signalosomes regulate central mechanisms underlying cell migration. *eLife*. 14:e08384. doi:10.7554/eLife.08384.
34. Chan PM, Lim L, Manser E. 2008. PAK is regulated by PI3K, PIX, CDC42, and PP2C α and mediates focal adhesion turnover in the hyperosmotic stress-induced p38 pathway. *J Biol Chem*. 283:24949–24961. doi:10.1074/jbc.M804917200. [PubMed: 18586681]
35. Chu J, Zhang J, Cao X, Li Y, Wang Z, et al. 2013. Biphasic regulation of myosin light chain phosphorylation by p21-activated kinase modulates intestinal smooth muscle contractility. *J Biol Chem*. 288:1200–1213. doi:10.1074/jbc.M112.439267. [PubMed: 23161543]
36. Arber S, Barbayannis FA, Hanser H, Schneider C, Stanyon CA, et al. 1998. Regulation of actin dynamics through phosphorylation of cofilin by LIM-kinase. *Nature*. 393:805–809. doi:10.1038/31642. [PubMed: 9655397]
37. Yang N, Higuchi O, Ohashi K, Nagata K, Wada A, et al. 1998. Cofilin phosphorylation by LIM-kinase 1 and its role in Rac-mediated actin reorganization. *Nature*. 393:809–812. doi:10.1038/31511. [PubMed: 9655398]
38. Gardel ML, Schneider IC, Aratyn-Schaus Y, Waterman CM. 2010. Mechanical integration of actin and adhesion dynamics in cell migration. *Annu Rev Cell Dev Biol*. 26:315–333. doi:10.1146/annurev-cellbio-100109-104028. [PubMed: 19575647]

39. Byrne KM, Monsefi N, Dawson JC, Degasperis A, Bukowski-Wills JC, et al. 2016. Bistability in the Rac1, PAK, and RhoA signaling network drives actin cytoskeleton dynamics and cell motility switches. *Cell Syst.* 2:38–48. doi:10.1016/j.cels.2016.06.012. [PubMed: 27136688]
40. Hauert AB, Martinelli S, Marone C, Niggli V. 2002. Differentiated HL-60 cells are a valid model system for the analysis of human neutrophil migration and chemotaxis. *Int J Biochem Cell Biol.* 34:838–854. doi:10.1016/S1357-2725(02)00010-9. [PubMed: 11950599]
41. Blanter M, Gouwy M, Struyf S. 2021. Studying neutrophil function in vitro: cell models and environmental factors. *J Inflamm Res.* 14:141–162. doi:10.2147/JIR.S284941 [PubMed: 33505167]
42. Yu Y, Luo W, Yang J, Zhang Y, Shu Y, Lu J, et al. 2018. miR-190 suppresses breast cancer metastasis by regulation of TGF- β -induced epithelial–mesenchymal transition. *Mol Cancer.* 17:70. doi:10.1186/s12885-018-0372-4 [PubMed: 29510731]
43. Xiong Y, Fang JH, Yun JP, Yang J, Zhang Y, Jia WH, et al. 2018. miR-190 promotes HCC proliferation and metastasis by targeting PHLPP1. *Exp Cell Res.* 371:185–195. doi:10.1016/j.yexcr.2018.07.004 [PubMed: 30092222]
44. Yu Y, Yang J, Li Q, Xu B, Lian Y, Miao L, et al. 2019. miR-190 enhances endocrine therapy sensitivity by regulating SOX9 expression in breast cancer. *J Exp Clin Cancer Res.* 38:22. doi:10.1186/s13046-019-0997-7 [PubMed: 30658681]
45. De Lella Ezcurra AL, Hernandez G, Errede M, Caceres A, Wappner P. 2016. miR-190 enhances HIF-dependent responses to hypoxia in *Drosophila* by inhibiting the prolyl-4-hydroxylase Fatiga. *PLoS Genet.* 12:e1006073. doi:10.1371/journal.pgen.1006073 [PubMed: 27223464]
46. Mattera R, Tsai YC, Weissman AM, Bonifacino JS. 2006. The Rab5 guanine nucleotide exchange factor Rabex-5 binds ubiquitin (Ub) and functions as a Ub ligase through an atypical Ub-interacting motif and a zinc finger domain. *J Biol Chem.* 281:6874–6883. doi:10.1074/jbc.M510595200 [PubMed: 16407276]
47. Lauer J, Segeletz S, Cezanne A, Kiontke S, Kummel D, Ungermann C. 2019. Auto-regulation of Rab5 GEF activity in Rabex5 by allosteric structural changes, catalytic core dynamics and ubiquitin binding. *eLife.* 8:e46302. doi:10.7554/eLife.46302 [PubMed: 31718772]
48. Zhang Z, Zhang T, Wang S, Gong Z, Tang C. 2014. Molecular mechanism for Rabex-5 GEF activation by Rabaptin-5. *eLife.* 3:e02687. doi:10.7554/eLife.02687 [PubMed: 24957337]
49. Zhu H, Zhu G, Liu J, Liang Z, Li G. 2007. Rabaptin-5-independent membrane targeting and Rab5 activation by Rabex-5 in the cell. *Mol Biol Cell.* 18:4119–4128. doi:10.1091/mbc.E07-02-0111 [PubMed: 17699593]
50. Jékely G, Sung HH, Luque CM, Rørth P. 2005. Regulators of endocytosis maintain localized receptor tyrosine kinase signaling in guided migration. *Dev Cell.* 9:197–207. doi:10.1016/j.devcel.2005.06.014 [PubMed: 16054027]
51. Hellberg C, Schmees C, Karlsson S, Åhgren A, Heldin CH. 2009. Activation of protein kinase C is necessary for sorting the PDGF-receptor to Rab4a-dependent recycling. *Mol Biol Cell.* 20:2856–2863. doi:10.1091/mbc.E08-07-0764 [PubMed: 19369415]
52. Christoforides C, Rainero E, Brown KK, Norman JC, Toker A. 2012. PKD controls α v β 3 integrin recycling and tumor cell invasive migration through its substrate Rabaptin-5. *Dev Cell.* 23:560–572. doi:10.1016/j.devcel.2012.07.009 [PubMed: 22975325]
53. Laufer JM, Hauser MA, Kindinger I, Purvanov V, Pauli A, Legler DF. 2019. Chemokine receptor CCR7 triggers an endomembrane signaling complex for spatial Rac activation. *Cell Rep.* 29:995–1009.e6. doi:10.1016/j.celrep.2019.09.031 [PubMed: 31644919]
54. Palamidessi A, Frittoli E, Garré M, Faretta M, Mione M, Testa I, et al. 2008. Endocytic trafficking of Rac is required for the spatial restriction of signaling in cell migration. *Cell.* 134:135–147. doi:10.1016/j.cell.2008.05.034 [PubMed: 18614017]
55. Schiefermeier N, Teis D, Huber LA. 2011. Endosomal signaling and cell migration. *Curr Opin Cell Biol.* 23:615–620. doi:10.1016/j.ceb.2011.04.001 [PubMed: 21546233]
56. Tebar F, Enrich C, Rentero C, Grewal T. 2018. GTPases Rac1 and Ras signaling from endosomes. In: Lamaze C, Prior I, editors. *Endocytosis and signaling*. Cham (CH): Springer International Publishing. (Prog Mol Subcell Biol; vol. 57). p. 65–105. doi:10.1007/978-3-319-96704-2_3

57. Wei F, Cao C, Xu X, Wang J. 2015. Diverse functions of miR-373 in cancer. *J Transl Med.* 13:162. doi:10.1186/s12967-015-0500-x [PubMed: 25990556]
58. Cortjens B, Van Woensel JBM, Bem RA. 2017. Neutrophil extracellular traps in respiratory disease: guided anti-microbial traps or toxic webs? *Pediatr Respir Rev.* 21:54–61. doi:10.1016/j.prrv.2016.11.006
59. Villanueva E, Yalavarthi S, Berthier CC, Hodgins JB, Khandpur R, Lin AM, et al. 2011. Netting neutrophils induce endothelial damage, infiltrate tissues, and expose immunostimulatory molecules in systemic lupus erythematosus. *J Immunol.* 187:538–552. doi:10.4049/jimmunol.1100326 [PubMed: 21613614]
60. Herrero-Cervera A, Soehnlein O, Kenne E. 2022. Neutrophils in chronic inflammatory diseases. *Cell Mol Immunol.* 19:177–191. doi:10.1038/s41423-021-00747-7 [PubMed: 35039631]

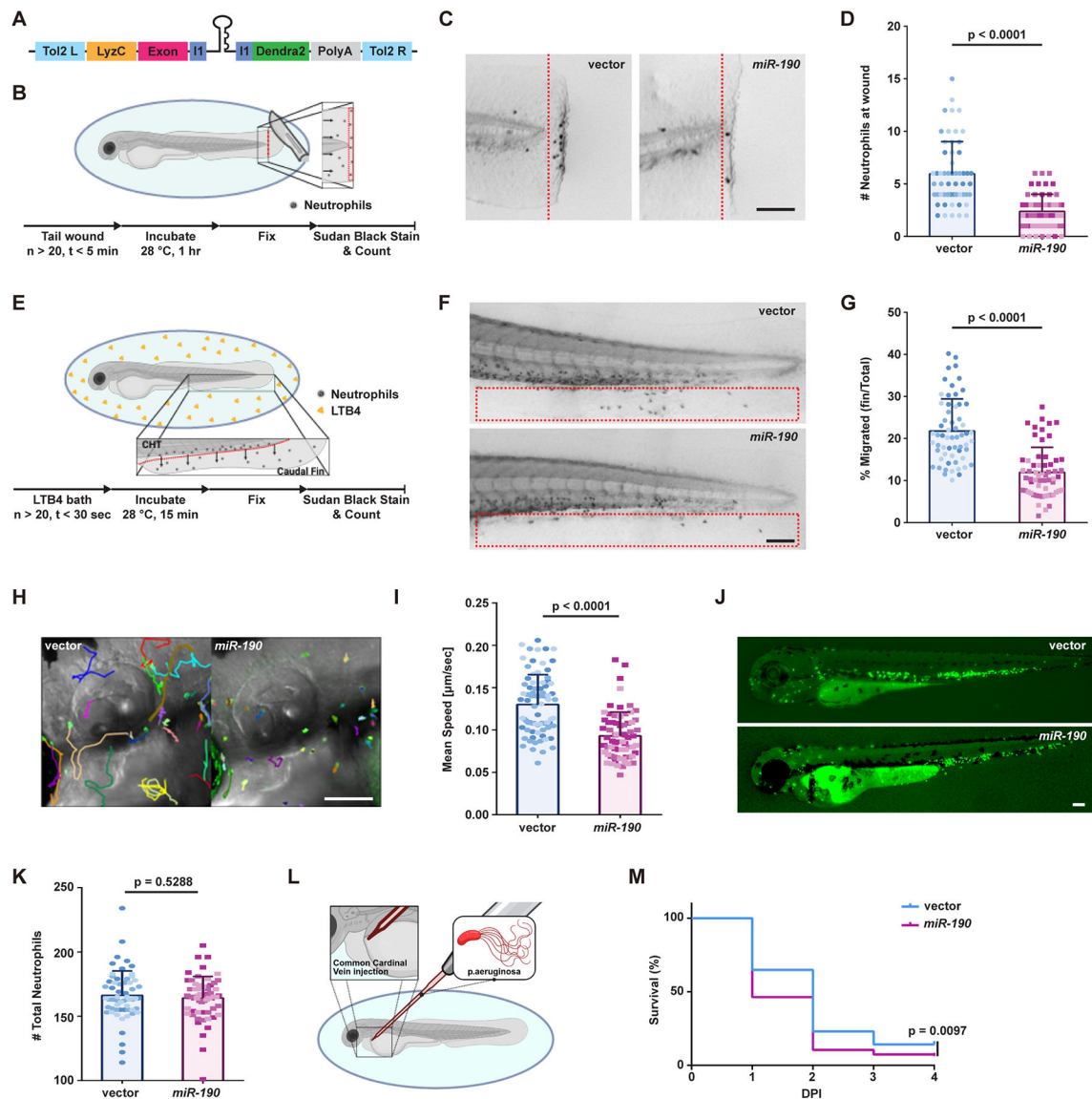


Figure 1. Overexpression of miR-190 in zebrafish neutrophils reduces cell motility and chemotaxis.

(A) Schematic of the Tol2-LyzC-miR-Dendra2 plasmid, injected into wild-type AB zebrafish embryos to generate *Tg(lyzC-miR-190-dendra2)^{pu38}* and *Tg(lyzC-vector-dendra2)^{pu7}* using the Tol2 transposon system. (B) Schematic of the zebrafish tail wounding assay showing Sudan black staining of wounded zebrafish to count neutrophils migrating to the wound at specific times after wounding. (C, D) Representative images and quantification of neutrophil recruitment. (Scale bar, 100 μ m) The assay included 3 biological repeats with 17-20 fish per group. Data are shown as mean \pm SD, analyzed with the Mann-Whitney test. (E) Schematic of the LTB4 chemotaxis assay showing Sudan black staining of zebrafish to measure the percentage of neutrophils migrating from the CHT to the caudal fin within specific times after LTB4 exposure. (F, G) Representative images and quantification of neutrophil chemotaxis from the CHT to the caudal fin in vector and miR-190 OE larvae after 15 min of LTB4 exposure. (Scale bar, 100 μ m) The assay included 3 biological repeats with

20 fish per group. Data are presented as mean \pm SD and analyzed using the Mann-Whitney test. (H, I) Representative images and quantification of live neutrophil motility in vector and miR-190 OE larvae over 30 min. (Scale bar, 100 μ m). The experiment included three biological repeats with 22-39 neutrophils tracked from 1 to 4 fish per group. Data are presented as mean \pm SD, and analyzed using the Mann-Whitney test. (J, K) GFP images and Sudan black staining quantifying whole-body neutrophils in vector and miR-190 OE larvae. (Scale bar, 100 μ m) The assay consisted of three biological repeats, with 20 fish per group. Data are shown as mean \pm SD, analyzed with the Mann-Whitney test. (L) Schematic of infection of the common cardinal vein with *P. aeruginosa*. (M) Survival analysis comparing miR-190 OE with vector controls. The experiment was repeated 3 times with a total of 95 miR-190 OE larvae and 91 vector control larvae. Data were analyzed using the Mantel-Cox test.

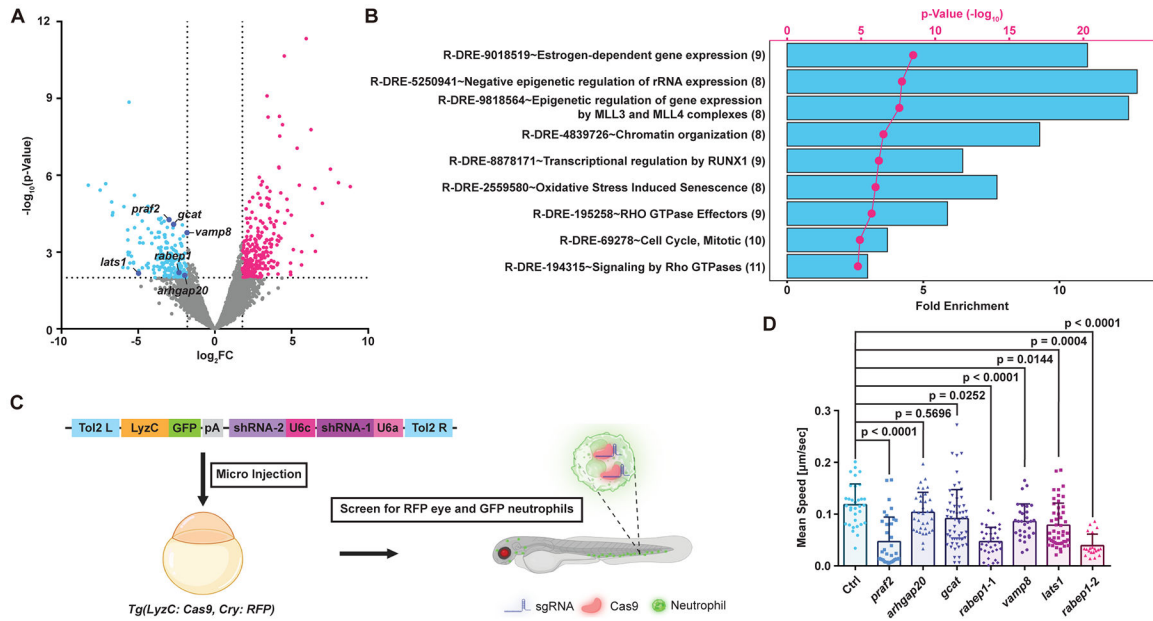


Figure 2. miR-190 overexpression significantly reduces rabep1 expression in neutrophils. (A) Volcano plot showing differentially expressed genes (DEGs) in miR-190 overexpressing (OE) neutrophils compared to vector controls. Down-regulated DEGs are depicted in cyan, and up-regulated DEGs in pink. Selected down-regulated DEGs based on screening criteria are highlighted in the plot. (B) GO enrichment analysis of significantly downregulated DEGs in miR-190-OE neutrophils. (C) Schematic of transient sgRNA-expressing plasmid injection into Cas9-expressing embryos to generate transient TSKO. sgRNA-expressing plasmids were designed to produce two separate sgRNAs targeting one specific gene at two different loci. (D) Quantification of neutrophil motility in transient TSKO screen. The assay included 3 biological repeats, each tracking 20-58 neutrophils from 5-8 fish per group. Data are presented as mean \pm SD and analyzed using Dunnett's multiple comparisons test.

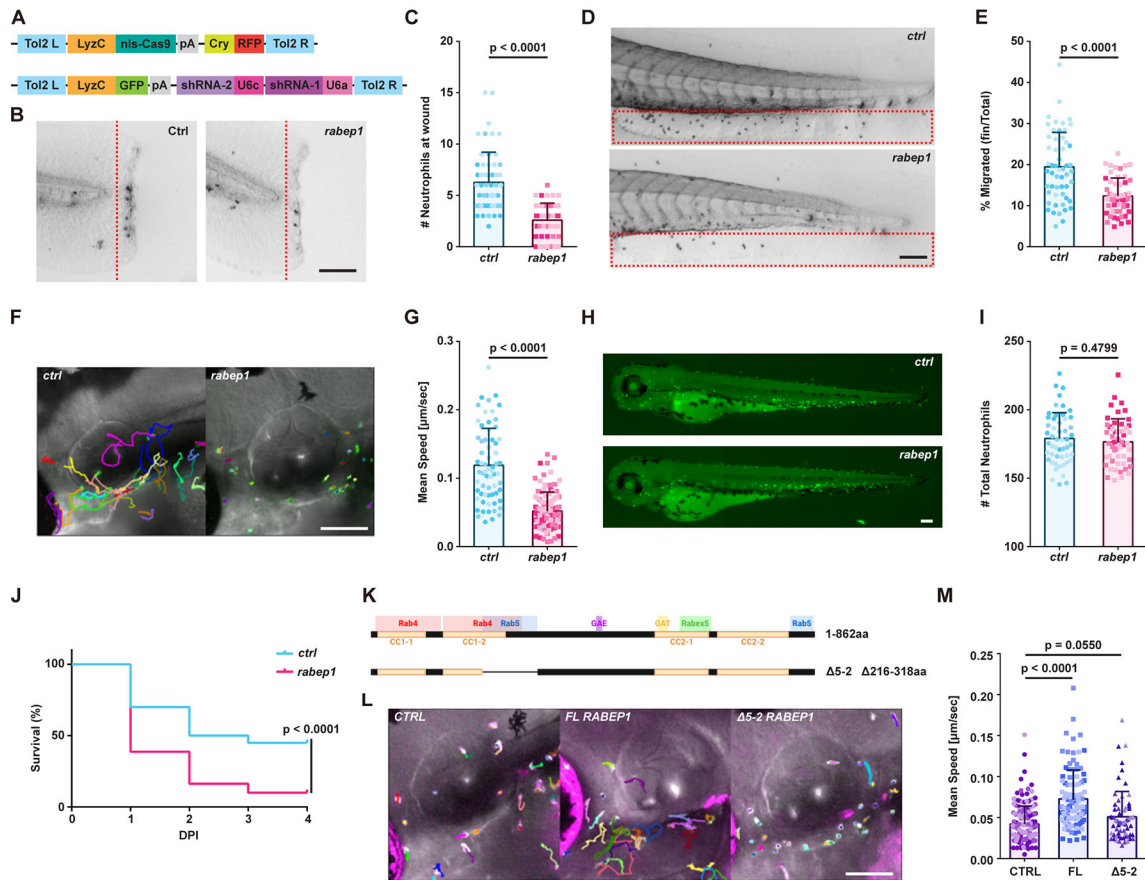


Figure 3. Knockout of Rabep1 in zebrafish neutrophils causes reduced cell motility and chemotaxis.

(A) Diagram of the Cas9-expressing plasmid and sgRNA-expressing plasmid used to create *rabep1* TSKO and control TSKO transgenic fish lines. (B, C) Representative images and quantification of neutrophil recruitment to the tail wound site in *Tg(LyzC: ctrl sgRNAs, LyzC: Cas9, Cry: RFP)* and *Tg(LyzC: rabep1 sgRNAs, LyzC: Cas9, Cry: RFP)* larvae 1 hour after wounding. Scale bar, 100 μ m. The experiment was performed with 3 biological repeats, each comprising 11-22 fish per group. Data are presented as mean \pm SD and analyzed using the Mann-Whitney test. (D, E) Representative images and quantification of neutrophil chemotaxis percentage from CHT to the caudal fin after 15 minutes of LTB₄ exposure in control TSKO and *rabep1* TSKO larvae. Scale bar, 100 μ m. The experiment was performed with 3 biological repeats, each with 16-20 fish per group. Data are shown as mean \pm SD, analyzed with the Mann-Whitney test. (F, G) Representative images and quantification of live neutrophil motility in control TSKO and *rabep1* TSKO larvae over 30 minutes. Scale bar, 100 μ m. The experiment was performed with three biological repeats, each tracking 19-38 neutrophils from three to four fish per group. Data are presented as mean \pm SD and analyzed using the Mann-Whitney test. (H, I) Representative GFP images and Sudan black staining quantification of overall neutrophil counts in control TSKO and *rabep1* TSKO larvae. Scale bar, 100 μ m. The experiment was performed with three biological repeats, each with 16-19 fish per group. Data are shown as mean \pm SD, analyzed with the Mann-Whitney test. (J) Survival analysis comparing *rabep1* TSKO with control TSKO. The

experiment included three biological repeats, totaling 80 *rabep1* TSKO larvae and 60 control TSKO larvae. Data are presented using the Mantel-Cox test. (K) Diagram of the full-length and 5-2 RABEP1 protein. (L, M) Representative images and quantification of neutrophil motility in larvae from *rabep1* TSKO crossed with Tol2-LyzC-RFP control, FL RABEP1 OE, or 5-2 RABEP1 OE over a 30-minute period. Scale bar, 100 μm . The experiment was performed with three biological repeats, each tracking 17-37 neutrophils from 2 to 4 fish per group. Data are presented as mean \pm SD and analyzed using Dunnett's multiple comparisons test.

Author Manuscript

Author Manuscript

Author Manuscript

Author Manuscript

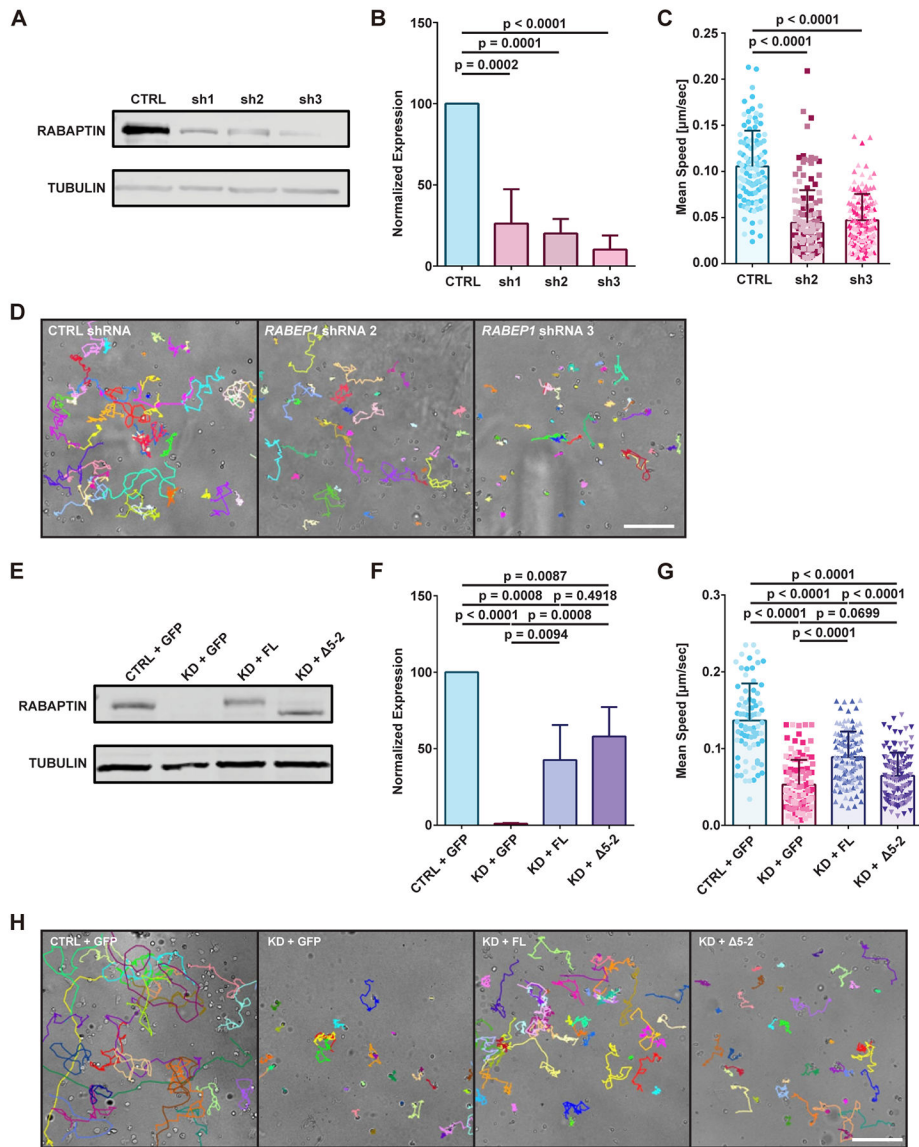


Figure 4. RABE1 is crucial for the motility of HL-60 cells.

(A, B) Representative images and quantification of immunoblots for RABAPTIN in control shRNA- and *RABE1* shRNA-expressing dHL-60 cells. TUBULIN serves as a loading control. The immunoblot was performed with three biological repeats, and quantification is shown as mean \pm SD, using Dunnett's multiple comparisons test. (C, D) Representative tracking images and quantification of the random migration of control shRNA or *RABE1* shRNA-expressing dHL-60 cells under agarose. Scale bar, 100 μm . The assay was conducted with three biological repeats, with 31-58 dHL-60 cells tracked per group. Data are presented as mean \pm SD, analyzed with Dunnett's test. (E, F) Representative images and quantification of RABAPTIN immunoblots in control shRNA with GFP control rescue, *RABE1* shRNA rescued with GFP control, full-length (FL) or $\Delta 5-2$ RABAPTIN in dHL-60 cells. TUBULIN was used as a loading control. The immunoblot included three biological repeats, and quantification is presented as mean \pm SD, with Dunnett's test. (G, H) Representative images

and quantified data of tracked random migration under agarose in the upper described groups. Scale bar, 100 μm . The assay involved three biological repeats, each tracking 24-48 dHL-60 cells per group. Data are shown as mean \pm SD, analyzed with Dunnett's multiple comparisons test.

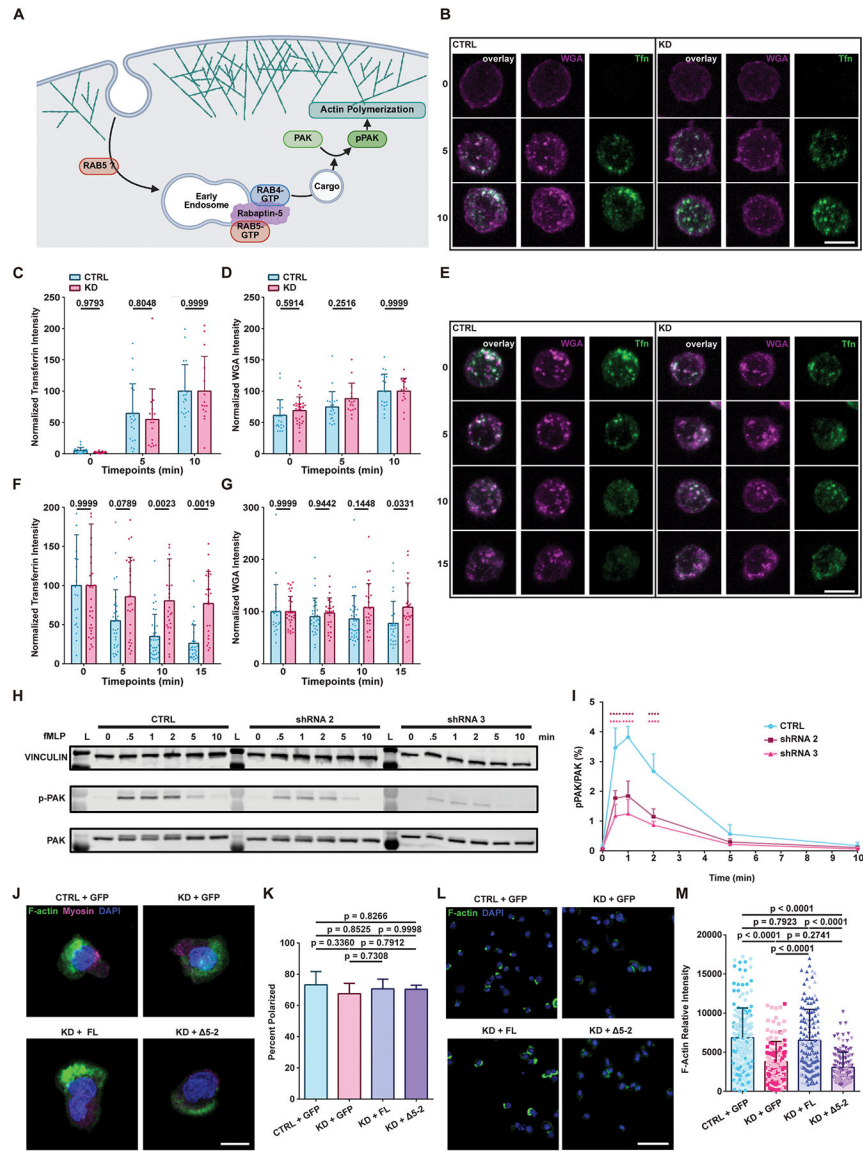


Figure 5. Rabaptin-deficient dHL-60 cells fail to recycle endosomes, induce PAK phosphorylation, and F-actin polymerization at the leading edge. (A) Schematic illustrating how RABEP 1 facilitates endosomal signaling to activate PAK, promoting actin filament formation at the leading edge. (B - D) Representative images and quantification of the internalization rates of Transferrin (Tfn) and WGA. Scale bar, 10 μ m. The average fluorescence intensity per cell was calculated and normalized to the 10-minute time point. The experiment included two biological repeats, each with 15- 31 cells per group at each time point. Data are shown as mean \pm SD, analyzed with Dunnett's multiple comparisons test. (E- G) Representative images and quantification of recycling rates of Tfn and WGA. Scale bar, 10 μ m. (C) The fluorescence intensity per cell was averaged and normalized to the 10-minute time point. (E)The fluorescence intensity per cell was averaged and normalized to the 0-minute time point. The assay was repeated twice with a total of 15-31 cells per group per timepoint. Data are presented as mean \pm SD, analyzed with Dunnett's test. (H, I) Representative images and quantitative immunoblot analysis of

PAK and pPAK in control and two separate *RABEP 1* knockdown dHL-60 cells after fMLP stimulation at the indicated timepoints. VINCULIN served as a loading control, and the ratio of pPAK to PAK expression was quantified. The immunoblot included three biological repeats, with data shown as mean \pm SD, analyzed by Dunnett's test. Significance levels are indicated by asterisks, where four asterisks denote $p < 0.0001$. (J, K) Representative images and quantification of polarization immunofluorescence staining in control, *RABEP 1* knockdown with GFP, FL, or 5-2 RABAPTIN expressing dHL-60 cells. Scale bar, 10 μ m. The experiment was performed twice, with 118- 226 cells in each group. Data are shown as mean \pm SD, analyzed with Dunnett's test. (L, M) Representative images and quantification of actin fluorescence intensity in the same group of cells. Scale bar, 50 μ m. Two biological replicates were conducted, with 31-35 cells per group. Data are presented as mean \pm SD, analyzed with Dunnett's test.

Table 1. The short list of putative *miR-190* target genes.

Gene Symbol	Full Gene Name	Accession	miR-190 Target Score	log ₂ FC	-log ₁₀ (p-value)
<i>prat2</i>	PRA1 Domain Family Member 2	NM_007213	-0.34	-2.629	4.365
<i>arhgap20</i>	Rho GTPase Activating Protein 20	NM_020809	-0.33	-1.503	0.896
<i>gcat</i>	glycine C-acetyltransferase	NM_001172554.1	-0.35	-2.601	5.289
<i>rabep1</i>	RAB GTPase binding effector protein 1	NM_004703	-0.32	-2.472	3.912
<i>vamp8</i>	Vesicle-associated membrane protein 8	NM_003761	-0.30	-1.965	3.323
<i>lats1</i>	large tumor suppressor kinase 1	NM_004690	-0.25	-4.803	1.768

Author Manuscript

Author Manuscript

Author Manuscript

Author Manuscript